Hindawi
Geofluids
Volume 2022, Article ID 8297754, 10 pages
https://doi.org/10.1155/2022/8297754

Research Article

Multifactor Analysis of Landslide Mechanisms: A Case Study of Yongji Expressway, China

Qingfeng Meng,[1,2] Xuyue Hu,[1] Jing Zhang,[2] Peng Li,[2] Chunguang Zhou,[2] and Zhi Wang[3]

[1]*School of Hydraulic Engineering, Changsha University of Science and Technology, Changsha 410114, China*
[2]*Zhongnan Engineering Corporation Limited Power China, Changsha 410014, China*
[3]*School of Mechanics and Safety Engineering, Zhengzhou University, Zhengzhou 450001, China*

Correspondence should be addressed to Peng Li; 02489@msdi.cn and Zhi Wang; wangzhi@zzu.edu.cn

Received 6 April 2022; Accepted 20 May 2022; Published 13 June 2022

Academic Editor: Zhengzheng Xie

Based on deformation monitoring and stability results obtained from geological mapping, geological drilling, macrolaboratory, and microlaboratory tests, the sliding mechanism of landslide in Guzhang County of Yongji expressway was studied. The bedding slope landslide results from cutting slope along the central white mud clay slip, and by on-site investigation and deep displacement monitoring, the clay is determined as the landslide surface. Combining the experimental results and similar geotechnical engineering experience, by back-calculation, the parameters of the soft interlayer are calculated as C(5 kPa) and ϕ (8.5°). Based on X-ray diffraction (XRD) and X-ray fluorescence spectroscopy (XRF) test, the results are concluded that the chlorite in clay interlayer is easily water softened, excavation slope after long-term heavy rainfall chlorite clay interlayer softening. Sustained rainfall and underground water levels showed a positive correlation when the slope is sliding, and the heavy rainfall continued to accelerate slope sliding. Furthermore, the slope surface displacement and profound displacement increase quickly, and rainfall and slope displacement also showed a positive correlation.

1. Introduction

The construction of mountain highways plays a vital role in promoting economic development in mountainous areas. However, geological disasters such as landslides and mudslides caused by underground engineering and other construction excavation often occur. Slope protection engineering has increasingly become an essential part of underground engineering safety. The study of landslides in mountainous areas with particularly complex geological conditions is of great significance for similar engineering construction and geological disaster prevention and control [1, 2].

Many studies on geological hazards are caused by engineering construction in mountainous areas, mainly focusing on stability analysis, deformation destabilization mechanism, and prevention and control technology research. Li et al. [3] from Institute of Geophysics, the Chinese Academy of Sciences, and Dai et al. [4] from the China University of Geosciences took large mountain landslides in the Three Gorges Hydropower Project reservoir area as the research object. They studied the internal and external dynamic coupling mechanism of geological disaster formation from three aspects: spatial distribution characteristics, development and evolution of slip zone, and nuanced geological analysis [3, 4]. Chang'an University and others selected the giant smooth rocky landslide in the Three Gorges reservoir area as the research object. They explored the physical and mechanical properties of the landslide geotechnical body and the landslide resurgence through indoor and outdoor physical and mechanical tests such as hydrochemical tests, X-ray diffraction tests, microstructure electron microscope scanning tests, and significant direct shear tests of the landslide soil based on geological surveys, flat caving, trenching, and borehole exposures, combined with the results of ESR dating tests and deformation monitoring. The intrinsic correlation between landslides' physical and mechanical properties and

landslide resurgence and instability was investigated [5–8]. The Chengdu University of Technology obtained the shear parameters of the sliding surface of the ancient landslide of the red-bedded rock body Miaoziyan by repeated shear tests, made stability calculations for various working conditions using the limit analysis energy method, and proposed antislip measures [9, 10]. The Chinese Academy of Railway Sciences summarized the characteristics and types of ancient landslides of a large number of highways in the mountainous areas of Fujian, proposed remediation countermeasures for each type of disease and the content and technical points of each stage of an investigation, and studied the method of evaluating the postwork effect of antislip pile remediation measures [11]. Chongqing Jiaotong University and Northeast Forestry University and other institutions took highway landslides as the research object, studied the effects of essential factors such as excavation, rainfall, and groundwater, and proposed suggested prevention and control measures [8, 9, 12–17].

In this paper, based on the preliminary survey and design, geological mapping, geological drilling, macrolab, and microlab tests, deformation monitoring, and stability analysis are used to study the sliding mechanism of the landslide in Yongji Expressway and to analyze and judge the potential sliding surface and form of instability of the slope from the perspective of engineering geology. It is aimed at identifying the geological engineering conditions within the slope area and providing the necessary geological basis for slope management design and construction.

2. Project Overview

Yongshun-Jishou Expressway (referred to as Yongji Expressway) is a critical interprovincial corridor in the northwestern region of Hunan Province, China. It is an essential part of the seventh column in the "seven vertical and nine horizontal" expressway network planning of Hunan Province. Yongji Expressway starts from Yongshun, passing through Furong Town, Luoyixi, Guzhang, Jishou City, and docking with Baomao Expressway, a crucial interprovincial corridor from the northwest Hunan Province to Hubei Province and a vital infrastructure to build a golden tourism corridor in western Hunan Province. The mainline of Yongji Expressway is 85.247 km long and passes through scenic spots with complex topography and geological conditions, which is a typical mountainous highway.

The ninth construction section of Yongji Expressway, i.e., mileage K40 + 500 to K40 + 906 (see Figure 1), basically extends along the slope of the mountain; the terrain is high on the left and low on the right, and the foot of the slope is Guzhang County, and four more extensive slopes are formed on the left after cutting; i.e., K40 + 500 to K40 + 584 is No. 1 slope, K40 + 584 to K40 + 672 is No. 2 slope, K40 + 672 to K40 + 748 is No. 3 slope, and K40 + 768 to K40 + 906 is No. 4 slope. According to the Chinese side slope classification, the largest of these four slopes is a grade 4 slope with 10 m grading and a maximum slope height of 39.5 m. As shown in Figure 1, slope No. 4 was significantly deformed when excavated to the foot of the grade 2 slope, and two more significant deformations occurred in August 2014 and January 2015, with a larger collapse volume (Crack No. 5, No. 6, and No. 4). There is no obstruction between the landslide and the city. Once a large-scale landslide occurs, the landslide will completely bury many buildings in the county, and the lives of tens of thousands of residents will be threatened, which has caused much concern. Slope No. 2 and slope No. 3 are both grade 4 slopes, and the above grade 4 slopes have been reinforced. When excavation continued to the foot of the grade 1 slope, the treadmill found that an extensive penetration pulls crack (Crack No. 2 and No. 3) and several small cracks (Crack No. 7) appeared on both side slopes after the opening line about 150 meters backward. Later, it was found that the large crack had penetrated to No. 1 side slope so that the large cracks at the trailing edge of the four continuous slope bodies were all through, posing a more significant threat to the life and safety of the residents Guzhang County below.

In order to identify the sliding surface of the slope and the relationship between slope displacement, groundwater level, and rainfall, the main monitoring sections a1-a1′, a2-a2′, a3-a3′, and a4-a4′, as shown in Figure 1. Surface displacement (GPS), deep displacement, rainfall, and groundwater level were mainly monitored.

3. Slope Engineering Geological Conditions

3.1. Basic Geological Conditions. The region is located in the Wuling Mountains. The topography of the survey area is high on the left and low on the right. And at the foot of the slope is the county town of Guzhang. The project route is a low and medium mountain hilly landform unit with significant topographic changes. Gully development, steep valleys, treacherous terrain, rivers, and valleys are mostly "V" type, the depth of the valley range between 50 and 130 m. Before the large-scale excavation of the site, the survey area was a ridge protruding toward the county town. After the slope excavation, except for local sections, it is mainly a cut square slope. Four higher slopes are formed on the left side, namely, No. 1, No. 2, No. 3, and No. 4 slopes shown in Figure 1; after site investigation, there are four continuous slope body rear edges of the large crack all through, posing a more significant threat to the life and safety of the residents of Guzhang County below.

Combined with the site investigation and drilling results, the stratigraphy of the site distribution from top to bottom is mainly the fourth series of powder clay, and the underlying bedrock is the slate of the Yuangujie Madi Group. Among them, the powder clay is a residual slope deposit, brownish yellow, rigid plastic, mainly composed of clay particles, containing vital weathering slate fragments, uneven content, varying compactness, thickness of 0 m~13.98 m, small thickness of excavation slope, and valley distribution, the large thickness of slope top distribution. The bedrock is slate of Madyi Formation in Yuangujie, purple-red in color, with variable structure and slab structure, mainly divided into solid weathering, medium weathering, and slight weathering: strong weathering cores are broken in the form of ruined blocks and gravels, with thickness of 0.81 m~17.70 m,

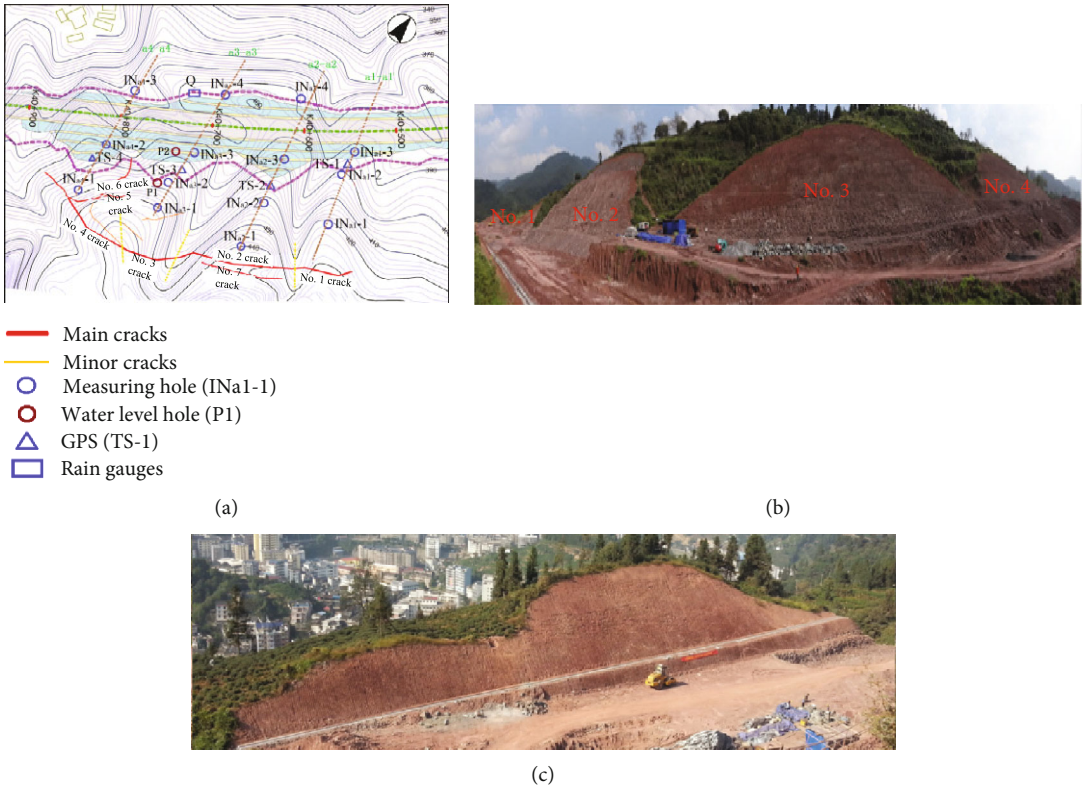

Figure 1: Slope topographic map: (a) monitoring section, (b) left side, and (c) right side.

generally distributed under the powder clay and exposed on the excavated slope; medium weathering is formed by slight metamorphism of siltstone, with hard rock quality, rock joints and fissures, and broken rock. The cores are mainly blocky and massive, and the rocks are complete at the local location, with thicknesses of 3.98 m~24.35 m. The micro-weathering is formed by slight metamorphism of siltstone, the upper part is purplish-red due to iron content, the rock is complex, and the hammering sound is crisp.

The project area is located in the broom-shaped arc tectonic zone of Xiangxi within the Wuling fold fault bundle of the Yangzi Quasi-Terrane of the Yangzi Block. The principal fracture structures in the region are the Luoyixi Fault and the Guzhang Reverse Fault. The Guzhang reverse fault is the most significant fracture structure affecting the survey area, which overlaps with the overall direction of Guyang River, with the fault tending to South-East and the dip angle of about 70°. The project area is located in the upper plate of the Guzhang reverse fault, and the project area is only 200 m-500 m away from the fault. The fault significantly affects the sloping rock, and the rock yield is complex and variable. According to the excavation, there is a minor reverse fault in the North-East direction on the left side of the lowermost slope near K40 + 720 in the slope area, which causes the rock formations on both sides of the fault to change sharply (Figure 2(a)) and thus has a significant impact on the formations and integrity of the slope rock body. According to China Earthquake Parameter Zoning Map (GB18306-2001), the peak acceleration of ground vibration in the project area is less than 0.05 g, and the characteristic period of ground vibration response spectrum is 0.35 s (the corresponding essential intensity of an earthquake is VI degree).

The project area belongs to the central subtropical monsoon humid climate, with prominent continental climate characteristics, warm winter and cool summer, four distinct seasons, long winter and summer, short spring, and autumn; abundant precipitation, annual rainfall of 1250~1500 mm, and rainfall concentrated in spring and summer, primarily seen in autumn drought. Groundwater in the area is mainly bedrock fracture water. Groundwater is mainly stored in the slate of Madyi Group of Panxi Group, with tectonic joints and fissures as the groundwater storage places.

3.2. Adverse Geological Conditions. Landslide is one of the main undesirable geological phenomena in the study area and is also the research object of this work. According to the geological survey and drilling data, the shallow layer of the slope is a slope residual soil layer with low strength; its lower part is firmly weathered slate with more developed joints and fissures and broken rock; the middle and lower parts are moderately weathered slate with high strength. The cover layer is mainly powder clay, unevenly containing a small amount of strongly weathered slate fragments. Atmospheric precipitation is easy to infiltrate along with this layer. The underlying bedrock is relatively watertight, so the surface cover layer is easy to produce landslides inside the cover layer or along with the base cover interface after the slope excavation. Secondly, the rock layer of the slope has a significant variation in yield, and when the rock layer tends

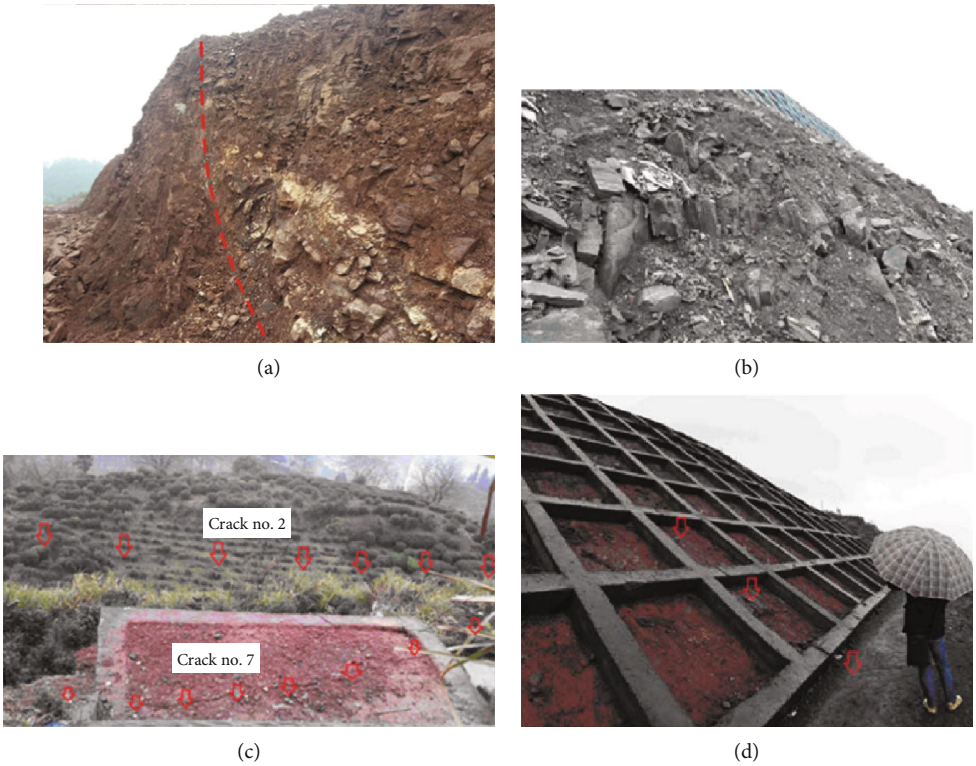

Figure 2: Deformation and cracks: (a) excavation reveals of the faults, (b) slope foot uplift, (c) main deformation crack, and (d) main deformation cracks of grid beam.

to be consistent with the slope direction and the dip angle is steep, it is easy to produce sliding along the layer, and the rock block of the slope is easy to produce sliding along the steeply inclined structural surface in the rock body. The block efficiently produces sliding along the steeply inclined structural surface in the rock body.

The upper part of the primary slope and the second slope above the primary slope of the right cutting slope are purple and purple-red powdery clay with fragmented rocks, and the underlying bedrock has a gentle yield, which should be ancient landslide accumulation from its genesis mechanism. From the excavation of the right side slope, a layer of white claystone is exposed at the bottom of the loose accumulation layer, and the bottom is strongly weathered slate with gentle production. The layer of claystone forms the boundary between the overburden and bedrock, and the structure of the overburden layer is loose, so it is a landslide accumulation (found near the middle of all four slopes), which should be the product of clay rock modification, and the overburden layer also has a loose structure. Therefore, the preliminary judgment is that this claystone layer is the suspected sliding surface of the ancient landslide.

3.3. Slope Deformation Features. One large crack and several small cracks appeared on the trailing edge of all four side slopes, which showed apparent slide pulling deformation. Taking the side slope from K40 + 584 to K40 + 674 as a typical illustration, when the side slope was excavated near the foot of the first grade, two major tension cracks appeared near the recess 146 m backward from the centerline of the roadbed (Figure 2(c)), and multiple tension cracks also appeared on the concrete grid beams on the second and third-grade slopes (Figure 2(d)), and the rock at the foot of the slope was elevated (Figure 2(b)).

As shown in Figure 2, two groups of cracks developed near the side slope notch, numbered Crack No. 2 and No. 7. Crack No. 2 (Figure 2(c)) is located 90 m beyond the opening line, with a visual depth of 2 m and a general width of 5~25 cm, and is connected to the side slope of small pile No. K40 + 500 to K40 + 584 in the left washout, and the large pile extends to the proper washout. Crack No. 7 is located 23 m above crack No. 2, visual depth 0.5 m, and the width of the crack is generally 3~10 cm. No. 2 crack form is high in the front and low in the back, the mountain is collapsed between crack No. 2 and No. 7, from the top of the left washout ditch where crack No. 2 is opened more expansive; we can see apparent concave and convex correspondence without noticeable friction marks.

Meanwhile, the front part of the No. 2 crack has apparent displacement relative to the back part toward the small pile number, and we can see crack No. 2 in the front part. It can be seen that the crack of No. 2 is caused by the front part of the mountain body pulling away from the roadbed direction and the direction of the small pile number. The cracks in the grid beam from the tertiary platform are perpendicular to the roadbed (Figure 2(b)), and the local reinforcement is pulled off, which also proves that the front of the mountain body has deformation in the lateral direction. The outward rise of the rock body from the middle and upper part of the primary slope (Figure 2(b)) also proves

that the mountain body has slid in the direction of the roadbed. The topographic map (Figure 1) shows that the ridge of the slope also runs in the direction of the minor stakes and intersects the roadbed diagonally. Therefore, the roadbed's excavation induced the hill's slide in the direction of the roadbed and the minor stakes.

4. Geotechnical and Physical Properties

4.1. Experimental Program. The suggested physical and mechanical property parameters for residual slope soil strongly weathered slate, moderately weathered, and below slate can be derived from the survey report, indoor tests, and experience of similar projects (see Table 1). The overburden soil plasticity index I_p is greater than 10 and less than 17, judged as powdered clay; liquidity index I_L is greater than 0 and less than 0.25, judged as a rigid plastic state. The saturation of Sr = 75.65% ~81.57% is wet, and the natural water content is low, which is judged to be medium to high compressibility soil. The uniaxial compressive strength of the rock masses ranges from 34.7 to 55.5 MPa, which is judged to be soft to hard rock and tends to increase with the depth of sampling.

After the field observation and physical test, it was found that the strength and hardness of the weak interlayer were no different from the surrounding rock under dry conditions. In contrast, the weak interlayer in a water-saturated state shows modification characteristics. After the rainfall, in situ samples (Table 2) were taken from the weak interlayer in the middle of the left and right slopes of the first grade of the four slopes. The weak interlayer soil's macroscopic physical and mechanical properties were determined by conventional geotechnical experiments (including straight shear and repeated shear).

In order to find out the mineral content and elemental content of the weakly interbedded soil, the specimens were dried and ground into powder and subjected to X-ray fluorescence diffraction (XRD) and X-ray fluorescence spectroscopy (XRF) tests. Then, the physical and mechanical properties were evaluated comprehensively.

4.2. Experimental Results and Analysis. The weak strata at different field numbered positions were sampled. The liquid limit, plastic limit, moisture content, shear strength, and internal friction angle of the soil were tested using a combined liquid limit plasticity tester and a geotechnical repeated direct shearing instrument. The physical and mechanical property test results of the weak interlayer soil are shown in Table 3, which shows that the test indexes of different specimens do not vary much, among which the plasticity index, I_p, is less than 10, which is a silty soil, the liquidity index, I_L, is greater than 0 and less than 1, which is a hard plastic to a soft plastic state. The saturation is close to 100%, which means the pores are full of water. Compression coefficients are more significant than 0.10 MPa^{-1} and less than 0.5 MPa^{-1} for medium compressibility soils, and the weak interlayer C (5 KPa~20 KPa) and ϕ (5.27° ~10.76°) obtained by straight shear and repeated shear. Combined with the experimental results and similar engineering experience, the range of weak interlayer soil parameters can be narrowed down to C' (5 KPa~8 KPa), ϕ' (8°~10°).

Table 1: Reference value of the physical and mechanical property parameters of residual slope soil.

Geotechnical type	γ (kN/m^3)	C (KPa)	ϕ (°)
Slope residual soil	21	12	27
Strongly weathered	23	25	30
Moderately weathered and below	24	45	35

Table 2: Sampling location of weak interlayer soil.

Field number	Location
a1-1	K40 + 500 ~ K40 + 584 Left side, first grade slope, middle location
a1-1	K40 + 500 ~ K40 + 584 Right side, first grade slope, middle location
a1-2	K40 + 500 ~ K40 + 584 Right side, first grade slope, middle location
a2-z1	K40 + 584 ~ K40 + 674 Left side, first grade slope, middle location
a2-y1	K40 + 584 ~ K40 + 674 Right side, first grade slope, middle location
a3-z1	K40 + 674 ~ K40 + 748 Left side, first grade slope, middle location

Table 3: Test results of weak interlayer soil.

Number	ω (%)	ρ (g/cm^3)	I_p	I_L	ϕ (°)	C (MPa)	ϕ' (°)	C' (MPa)
a1-1	23.64	2.09	8.51	0.70	8.53	0.010	6.57	0.009
a1-1	22.10	2.03	9.16	0.75	6.84	0.008	5.27	0.007
a1-2	22.05	1.98	9.39	0.80	7.97	0.014	6.14	0.012
a2-z1	21.67	2.07	8.60	0.23	6.84	0.020	5.27	0.017
a2-y1	20.89	1.97	9.02	0.06	10.76	0.009	8.29	0.008
a3-z1	22.30	1.82	9.59	0.35	7.97	0.006	6.14	0.005

Table 4: The contents of main mineral composition (XRD).

Mineral	Quartz	Mica	Chlorite	Hematite and others
Content (%)	70	15	10	5

The results of X-ray fluorescence diffraction (XRD) and X-ray fluorescence spectroscopy (XRF) analysis tests are shown in Tables 4 and 5. It can be seen that the main components of the soft interlayer are quartz (S_iO_2), mica (S_iO_2 and $A_{l2}O_3$), and chlorite (compounds containing Al, M_g, F_e, M_n, N_i, Z_n, and C_r). The properties of quartz and mica do not change much when they encounter water, while chlorite has softening properties when it encounters water (strength and hardness meet engineering requirements under dry conditions). We have done many experiments (uniaxial and triaxial compression experiments in dry and saturated states) on the softening properties of chlorite in water and found that the strength of the rock in the dry state

is much higher than that in the saturated state. The elastic modulus is also much higher than that in the saturated state. Further analysis concluded that the effect of chlorite-containing interlayer on the strength and stability of the sloping rock is divided into two stages according to the different effects of water on it (bilayer theory and pore pressure effect).

4.2.1. Phase I. When the weak interlayer is not exposed to water for a long time, its strength changes very little. After the slope excavation, the original drainage joints in the slope are destroyed. The fracture water flows to the interlayer at the foot of the slope (still relatively intact), and the interlayer is exposed to water for a long time. The interlayer is still relatively intact and less affected by the pore pressure, while the interlayer is mainly affected by the double electric layer (fixed and diffusion layers). The thicker the double electric layer is, the less the cohesion and friction between mineral particles. It should be explained that the fixed layer is the electrostatic gravitational effect of the mineral particles on the surrounding cations, while the diffusion layer acts just the opposite, formed by the diffusion force of Brownian motion.

According to the double layer theory (Equation (1)), the double-layer thickness $1/K$ is proportional to the ion concentration n_0. When the corresponding slope interlayer changes from dry to long-term contact with water, n_0 decreases significantly, so the thickness $1/K$ of the double electric layer increases significantly, and the adhesion and friction between mineral particles decrease.

$$\frac{1}{K} = \frac{1}{ev}\left(\frac{DkT}{8\pi\pi_0}\right)^{1/2}, \tag{1}$$

where $1/K$ is the thickness of the double layer; D is the dielectric constant; k is the Boltaz-Mann constant (1.38×10^{-23} J/K); T is the temperature (in K); e is the unit electronic charge (16.0×10^{-20}G); and n_0 is the expected concentration of ions (in ions/cm^3) in an aqueous solution far from the surface of the mineral particle.

4.2.2. Phase II. After the slope slides along the interlayer, the interlayer is sheared, and the overall porosity increases. In addition to the double electric layer effect, the pore pressure effect increases, further reducing the parameters of the interlayer. The slope continues to deform, the interlayer continues to be sheared, and the particles are ground up and further muddied.

4.3. Slope Deformation Monitoring. Surface displacement monitoring, deep displacement monitoring, rainfall monitoring, and groundwater level monitoring are used to realize the safety warning of the slope, and the internal relationship of each monitoring element is also studied. With the position of the sliding surface monitored by the slope measurement holes and the trend of change, it is judged that the sliding deformation occurred along a weak interlayer in the deep part of the slope. The shear outlet is the weak interlayer in the middle and lower part of the first-grade slope that the sliding surface shear outlets of the other three slopes are also located in the middle of the primary slope.

The surface displacement, deep displacement, rainfall, and groundwater level monitoring are shown in Figures 3 and 4. According to the deep displacement (Figure 5), it can be seen that there are apparent displacement mutations at 44 m, 36 m, and 15 m for holes IN_{a2}-1, IN_{a2}-2, and IN_{a2}-3 on the upper slope, respectively. Based on the location of the trailing edge fractures, the cores revealed by the boreholes (the location of the abrupt change corresponds to the white interlayer), the position of the sliding surface monitored by the slope measurement holes, and the trend of change, it is judged that the sliding deformation occurred along a weak interlayer in the deep part of the slope. The shear outlet is the weak interlayer in the middle and lower part of the first-grade slope, as predicted in Section 4.2. The direction is 340° to 360°, perpendicular to the primary fracture in Figure 6. Note that the sliding surface shear outlets of the other three slopes are also located in the middle of the primary slope, further verifying the sliding surface locations predicted in Section 4.2.

As seen in Figures 3 and 5, surface displacement monitoring point TS-3 is located between holes IN_{a3}-2 and IN_{a3}-3, and TS-3 displacement (60 mm) is also between hole IN_{a3}-2 (70 mm) and hole IN_{a3}-3 (28 mm) orifice displacement, and surface displacement and deep displacement are complementary to each other for verification.

The relationship graph between rainfall and groundwater level (Figure 4) shows that continuous heavy rainfall (100 mm daily) and groundwater level are positively correlated between May 13 and June 2.

From May 8 to May 15, the substantial continuous rainfall accelerated the slope sliding, prompting the slope surface displacement (Figure 3) and deep displacement (Figure 5) to increase at a more significant rate, and the rainfall and slope displacement showed a positive correlation under the critical condition.

4.4. Slope Stability Analysis. For a soil slope vulnerable failure, it can be assumed that the sliding mass has a circular slip surface with rotational geometry, as shown in Figure 7. According to the simplified Bishop's limit equilibrium method [17], the forces acting on a typical slice, ith slice, are as shown. The relationship between the normal force, N_i, and the mobilized shear resistance, T_i, can be written as

$$T_i = \frac{\left(C' l_i + N_i \tan \phi'\right)}{F_S}, \tag{2}$$

where C' and ϕ' are effective soil shear strength parameters, σ_i is normal stress, τ_i is shear stress, and $N_i = \sigma_i l_i$, $\tau_i = (C' + \sigma' \tan \phi')/F_S$, $T_i = \tau_i l_i$.

Resolving Equation (2) vertically, we have

$$N_i \cos \alpha_i = W_i + X_i - X_{i+1} - T_i \sin \alpha_i. \tag{3}$$

Table 5: The contents of main elements (XRF).

Element	O	S_i	A_l	K	N_a	M_g	F_e	Others
Content (%)	45.8	24.68	14.64	3.618	0.22	0.844	2.688	0.1098

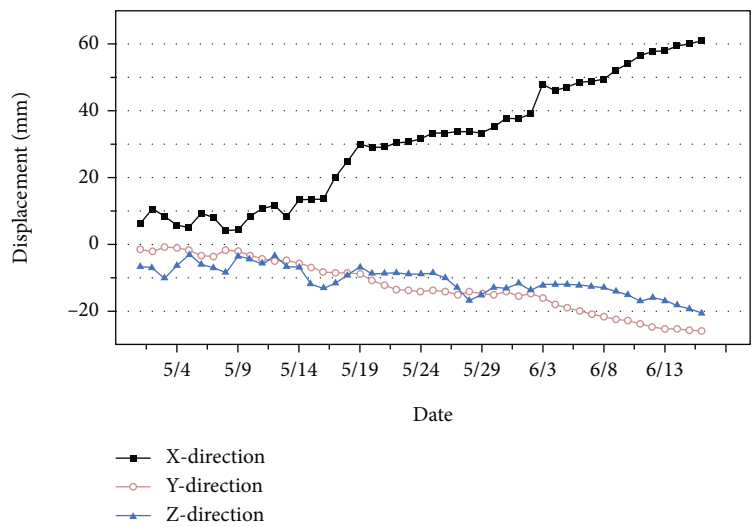

Figure 3: Slope surface displacement (K40 + 674 ~ K40 + 748).

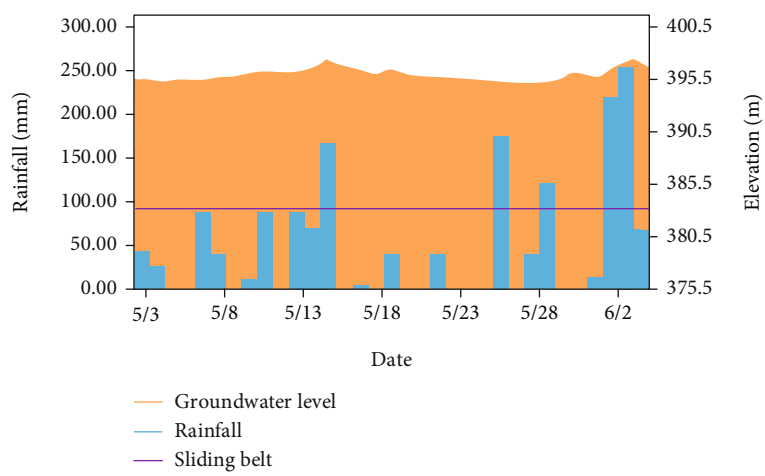

Figure 4: The rainfall and groundwater level monitoring map (P1 hole).

Solving Equations (3) and (4) together, we have

$$N_i = \frac{\left(W_i + X_i - X_{i+1} - \left(C' l_i / F_S\right) \sin \alpha_i\right)}{\xi_i}, \quad \xi_i = \cos \alpha_i + \frac{\sin \alpha_i \tan \phi'}{F_S}. \tag{4}$$

Stability coefficients can be solved according to torque equilibrium conditions when a slide mass is in ultimate equilibrium. When the slide mass is in a static-force ultimate equilibrium state, the sum of torques of vertical slices on the rotation axis of the slide mass is zero, namely,

$$\sum W_i x_i - \sum T_i R + \sum Q_i e_i = 0, \tag{5}$$

where W_i is the gravity of a slice, x_i is the horizontal distance from the vertical slice center to the rotation axis of the slide mass, T_i is the shearing resistance on the sliding bottom surface, R is the radius of the sliding surface, Q_i is the resultant radial force of circular soil lateral pressure, and e_i is the vertical distance from the application point of the resultant radial force of circular soil pressure to the rotation axis of the slide mass.

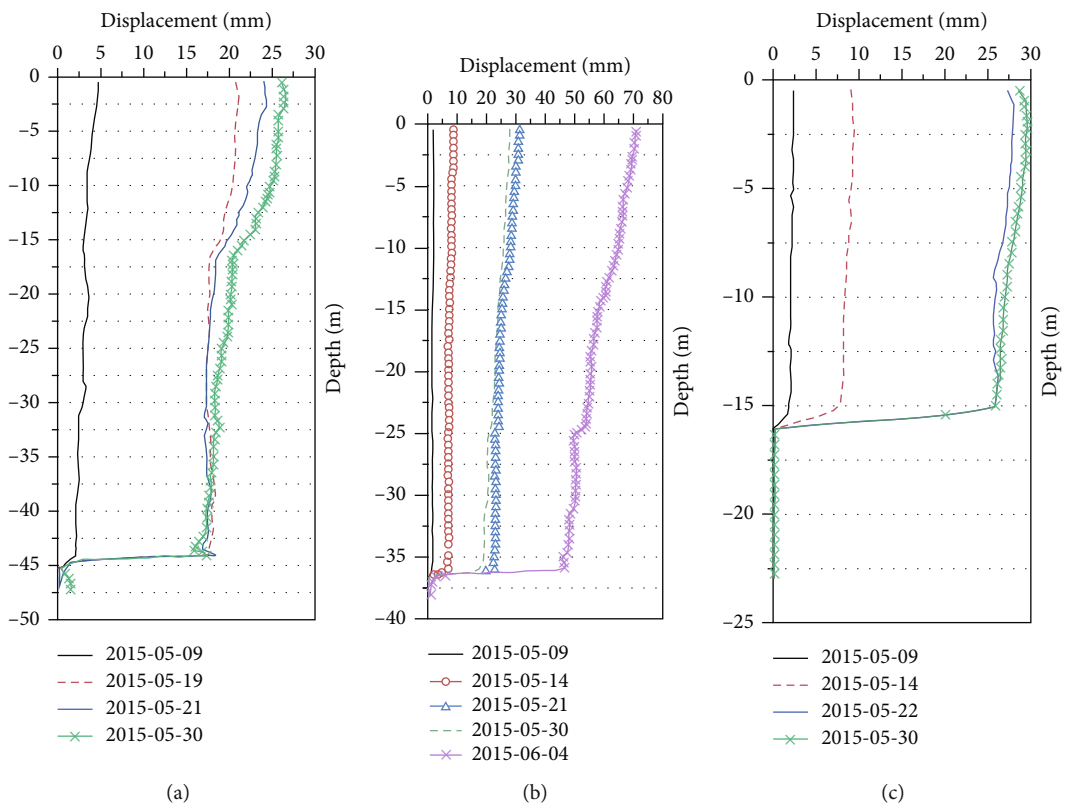

Figure 5: Deep displacement: (a) IN_{a3}-1 hole, (b) IN_{a3}-2 hole, and (c) IN_{a3}-3 hole.

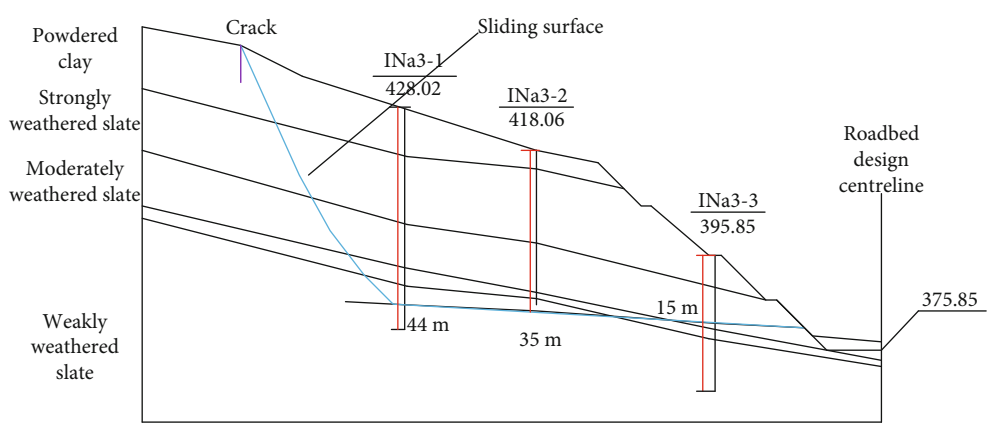

Figure 6: Engineering geological profile a3-a3′.

Combining Equations (3), (4), and (5), we have

$$F_S = \frac{\sum \xi_i \left[C' b_i + (W_i + X_i - X_{i+1}) \tan \phi' \right]}{(\sum W_i \sin \alpha_i + \sum Q_i e_i / R)}. \quad (6)$$

The simplified Bishop method assumes horizontal interslice forces, i.e., $X_R = X_L = 0$. Accordingly, Equation (6) can be expressed as

$$F_S = \frac{\sum \xi_i \left[C' b_i + W_i \tan \phi' \right]}{(\sum W_i \sin \alpha_i + \sum Q_i e_i / R)}. \quad (7)$$

The safety factor cannot be derived directly from Equation (7) and needs to be solved iteratively using the trial method. In this paper, the SLIDE calculation and analysis software is used to carry out a two-dimensional limit equilibrium analysis of the stability of the slope. According to the current deformation condition and development trend of the slope, the calculated safety factor of the a2-a2′ profile should be 0.99~1.02. After trial calculation, the parameters of the weak interlayer are determined as C (5 KPa) and ϕ (8.5°). The safety factor of profile K 40 + 640.0 within the No. 2 slope is 1.007 (see Figure 8). It can be seen that the calculation result is consistent with the actual situation and further verifies the reliability of the calculated parameters.

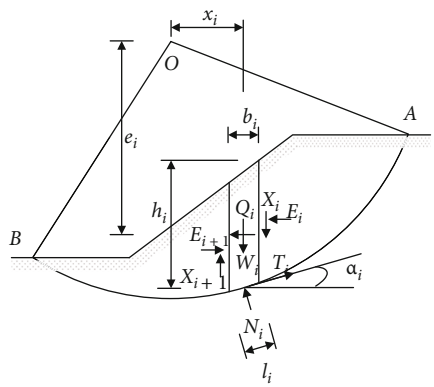

Figure 7: Schematics of Bishop's method.

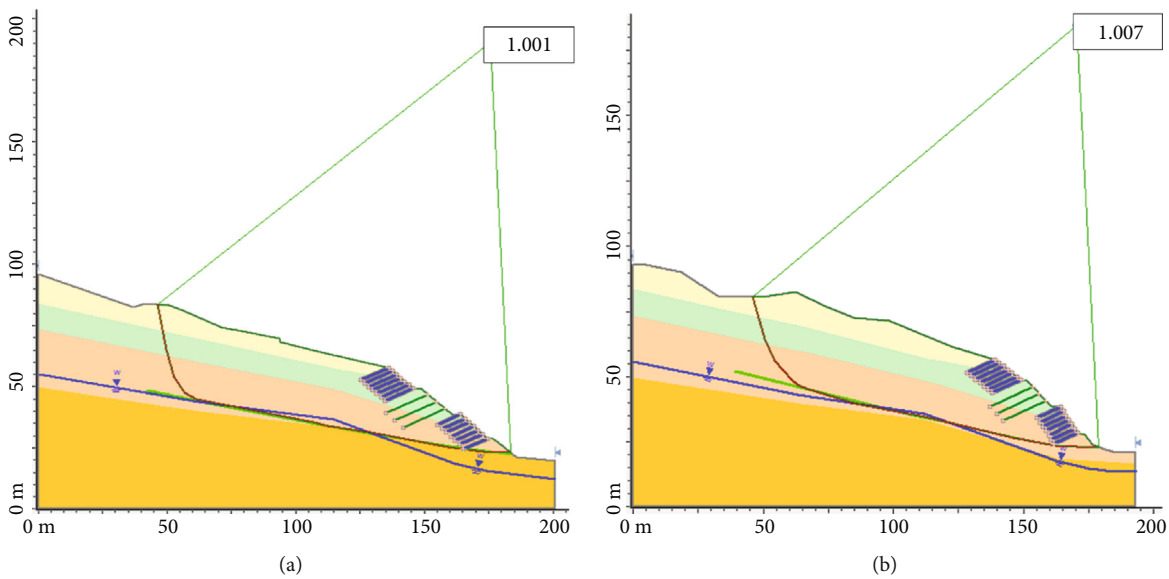

Figure 8: Calculation result of SLIDE: (a) section a1-a1′; (b) section K40 + 640.0.

The landslide mechanism is affected by many factors. Landslide prevention needs to be dealt with separately according to the different influence weights. The reduction of load, the construction of a drainage system, the addition of support structures, and the reinforcement of bolts are considered effective measures to reduce the occurrence of landslides. This case is a typical resurrection case of an ancient landslide group. The landslide mechanism is affected by many factors, e.g., groundwater and geological structure, through theoretical analysis, laboratory tests, field measurement, and other means to find the principal elements and use parameter inversion. Another means to analyze the safety of landslides is an essential means of ancient geological landslide design, which has a vital reference significance for the creation of engineering excavation schemes in the ancient landslide area.

5. Conclusions

In this study, a combination of field observations, laboratory analyses, and theoretical calculations was used to investigate the slopes of Guzhang County on the Yongji Expressway, and numerous raw test data were obtained to reveal the sliding mechanism of the landslide and to verify it. Based on the obtained results, the following conclusions can be drawn:

(1) The landslide in Guzhang County of Yongji Expressway was caused by the excavation of a cut-to-square slope and the sliding of the bedding slope along the middle of the first-grade slope with white marginalized clay. The interlayer was between the upper loose deposits and the underlying strongly weathered slate. It is the product of clay rock argillaceous, and it is comprehensively determined that this layer of clay rock is the sliding surface of the ancient landslide body through on-site investigation and deep displacement monitoring

(2) Combined with the geotechnical experiment results and similar engineering experience, the parameters of the weak interlayer were determined as C (5 KPa) and ϕ(8.5°) after back-calculation. Based on the results of X-ray fluorescence diffraction (XRD) and X-ray fluorescence spectroscopy (XRF) tests, it

was concluded that the chlorite in the muddied interlayer encountered water softening characteristics, and the substantial long-term rainfall after excavation of the slope led to the softening of the chlorite-containing muddied interlayer

(3) When the slope is in a state of close sliding, the continuous heavy rainfall and groundwater level show a positive correlation, and the continuous heavy rainfall accelerates the sliding of the slope, prompting the surface displacement and deep displacement of the slope to increase at a more significant rate, and the amount of rainfall and slope displacement also show a positive correlation

Data Availability

The datasets and materials used and/or analyzed during the current study are available from the corresponding authors on reasonable request.

Conflicts of Interest

The authors declare that they have no known competing financial interests or personal relationships that could have appeared to influence the work reported in this paper.

Acknowledgments

This research was funded by the Huxiang Young Talent Project (Grant No. 2020RC3090), the R&D Project of Zhongnan Engineering Corporation Limited of Power China (Grant Nos. SQ-KJYF-2021-0137-03 and YFHT-1944), and the R&D Project of Department of Water Resources of Hunan Province (Grant No. 2-2021-04426).

References

[1] C. M. Lo, C. F. Lee, and W. K. Huang, "Failure mechanism analysis of rainfall-induced landslide at Pingguang stream in Taiwan: mapping, investigation, and numerical simulation," *Environmental Earth Sciences*, vol. 75, no. 21, pp. 1–20, 2016.

[2] L. Zhu, Y. Deng, and S. He, "Characteristics and failure mechanism of the 2018 Yanyuan landslide in Sichuan, China," *Landslides*, vol. 16, no. 12, pp. 2433–2444, 2019.

[3] X. Li, S. Li, and J. Chen, "Internal and external dynamic coupling mechanism of geological hazard," *Chinese Journal of Rock Mechanics and Engineering*, vol. 27, no. 9, pp. 1792–1806, 2008.

[4] Z. Dai, Y. Yin, and Y. Wei, "Study on failure mechanism of large deformation of ou'tang landslides in the Three Gorges Reservoir," *Journal of Engineering Geology*, vol. 24, no. 1, pp. 44–55, 2016.

[5] X. L. Hu, M. Zhang, M. J. Sun, K. Huang, and Y. Song, "Deformation characteristics and failure mode of the Zhujiadian landslide in the Three Gorges Reservoir, China," *Bulletin of Engineering Geology and the Environment*, vol. 74, no. 1, pp. 1–12, 2015.

[6] Y. Yin and Y. Wu, "Comprehensive study on a special ancient landslide in Three Gorges Reservoir Area," *The Chinese Journal of geological hazard and control*, vol. 9, no. S1, pp. 204–210, 1998.

[7] S. W. Sun, F. Q. Chen, and W. Wang, "Mechanism and remediation of a seismically induced landslide with a potential for deep seated sliding," *Soil Mechanics and Foundation Engineering*, vol. 52, no. 3, pp. 155–162, 2015.

[8] D. V. Chen, J. Xiong, and Y. F. Cui, "Back analysis of a debris landslide based on a real-time video recording: sliding process and post-slide investigation," *Bulletin of Engineering Geology and the Environment*, vol. 75, no. 2, pp. 647–658, 2016.

[9] Z. Wang, M. Xu, and S. Yang, "Landslide stability research of red rock on Wawushan Hydropower Station Powerhouse Area," *Journal of Engineering Geology*, vol. 19, no. 2, pp. 213–218, 2016.

[10] Y. Zhang, X. Wang, and Y. Liu, "Formation mechanism and stability analysis of a right abutment reservoir landslide in Sichuan," *Journal of Engineering Geology*, vol. 17, no. 3, pp. 335–342, 2009.

[11] L. Zhang and X. Liao, "Causes and treatment measures of bachimen landslide along Fuzhou-Ningde expressway," *Subgrade Engineering*, vol. 1, pp. 172–174, 2011.

[12] H. Zhu, H. Tang, and M. Li, "Study on stability analysis and control measures of Chongqing - Guizhou Expressway Xiang-Jia slope landslide," *Chinese Journal of Rock Mechanics and Engineering*, vol. 25, no. S1, pp. 2687–2693, 2006.

[13] G. H. Zhao, S. Wei, and J. Hua, "Landslide deformation monitoring and analysis of influence factors at K178 + 530 of the Bei'an to Heihe expressway," *Landslide Science for a Safer Geoenvironment*, vol. 3, pp. 503–510, 2014.

[14] F. S. Ma, Z. L. Li, and J. Wang, "Monitoring and engineering geology analysis of the Zhangmu landslide in Tibet, China," *Bulletin of Engineering Geology and the Environment*, vol. 76, pp. 855–873, 2017.

[15] C. D. Li, H. M. Tang, X. L. Hu, and L. Wang, "Numerical modelling study of the load sharing law of anti-sliding piles based on the soil arching effect for Erliban landslide, China," *KSCE Journal of Civil Engineering*, vol. 17, no. 6, pp. 1251–1262, 2013.

[16] X. N. Wang, "Geological properties of large-scale highspeed landslides and their mechanism models," *Bulletin of the International Association of Engineering Geology*, vol. 43, no. 1, pp. 93–99, 1991.

[17] J. Ji, W. Zhang, and F. Zhang, "Reliability analysis on permanent displacement of earth slopes using the simplified Bishop method," *Computers and Geotechnics*, no. 117, article 103286, 2020.